Induction Heating Specialized Simulation Software Adoption Benefits

How computer modelling can save company's time and money, and increase production efficiency

CENOS has already demonstrated that simulation software can be both affordable - by utilizing open-source tools, and easy-to-use - by building industry specialized apps with only relevant and easy-to-learn functionality. But there are still doubts to be clarified - what is the potential **return on the investment** and the **accuracy of simulation**. The goal of this whitepaper is to fill in the knowledge gaps.

What is CENOS?

CENOS is a finite element method (FEM) based computer-aided engineering (CAE) desktop software. CENOS Induction Heating application is designed for low- and medium-frequency induction heating calculation, it couples electromagnetic and thermal calculation algorithms to cover the full spectrum of induction-heating-related problems. CENOS allows 2D, axial symmetric, and 3D models for induction heating, pre-heating, hardening, brazing, annealing, tempering, and other processes for heating of various materials, such as steel, aluminum, copper, titanium, different alloys, and other electrically conductive materials. CENOS Induction Heating application can also simulate solely electromagnetic (steady-state, harmonic, or transient), solely thermal (steady-state or transient), and resistive heating tasks.

2. Simulation Accuracy Validation

GH Induction - Hardening And Tempering Of Pinion Shaft

The hardening installation lab test was carried out by Bernabé Núñez and Blas Barragán at GH Group Applications laboratory.

The actual workpiece in the manufacturing line (a small splined pinion shaft from gearbox) is rotated 400 revolutions per minute, it's heated up very quickly via induction and hardened in varying depth.

GH simulated the same heating process with CENOS simulation software. GH results revealed a higher temperature than projected - around 1200˚C which is completely acceptable. With rotation cases, the most important role is played by parameters like simulation time step and material properties.

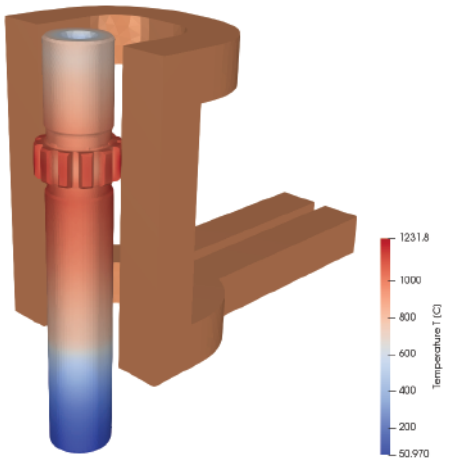

CENOS simulation results in 3D

The hardening installation lab test was carried out by Bernabé Núñez and Blas Barragán at GH Group Applications laboratory.

Elements	Configuration
GEN1	GEN 50 KW
TC	TC 20/1
TA	na
C	8 x 1uF

Parameters	Values
Power (Kw)	15
Frequency(Khz)	250
Voltage (V)	-
Current (A)	90
Regulation %	70
Inductor pressure(bar)	15
Inductor flow.(l/m)	12
Heating time	0,7 (+0,2 Q.Advance)
Rotation speed	400 rpm
Workpiece material	AISI 1045 (medium carbon steel)

Actual workpiece cros-section

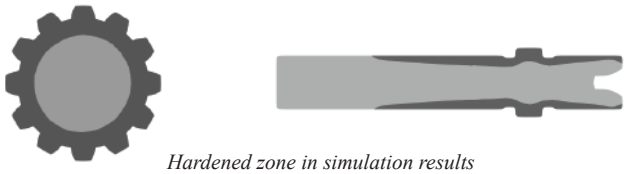

Hardened zone in simulation results

Temperature in simulation results

GH wanted to compare the hardening depth of two cases - one from simulation and one from the factory. Images show that the range of depth is between 0.3-2.0 mm, just as they were expecting. Thus, the simulation accurately predicted lab results.

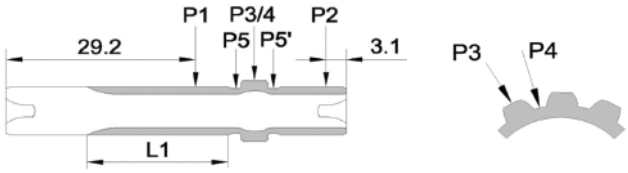

Hardening depth measurements

Measurement	Acceptable range	CENOS results
P1	0,3 - 2,0 mm	1,19 mm
P2	0,3 - 2,0 mm	0,36 mm
P3	0,3 - 2,8 mm	1,73 mm
P4	0,3 - 2,0 mm	1,17 mm
P5	0,3 - 2,0 mm	1,17 mm
P5'	0,3 - 2,0 mm	0,99 mm
L1	min 15 mm	19,3 mm

SMS Elotherm - Hardening

This validation case was carried out by SMS Elotherm induction heating engineer Judith Levermann.

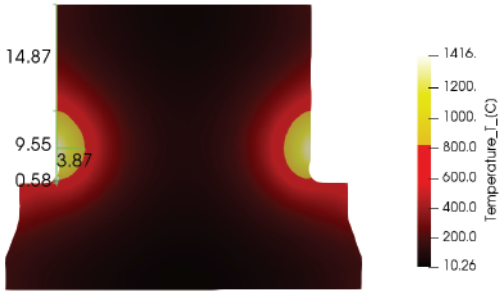

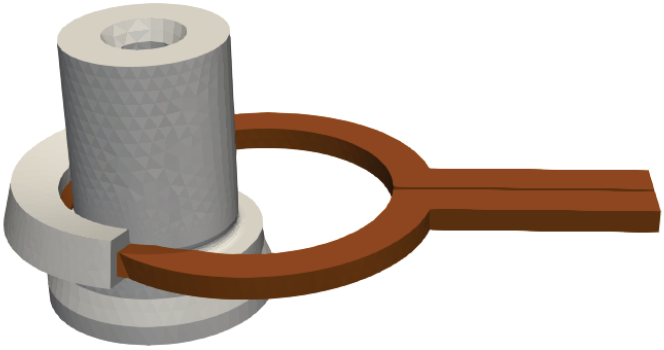

Inductor with magnetic concentrator made from laminated steel sheets

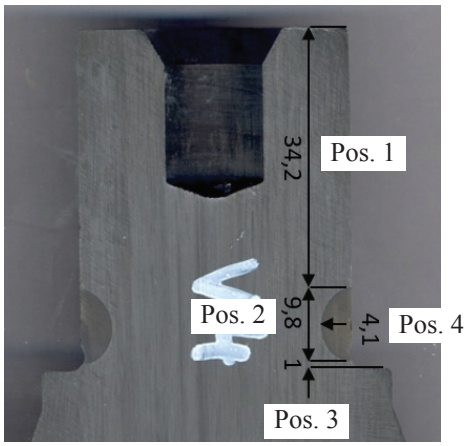

Calculation

The first task was to determine the best workpiece and magnetic concentrator material. Three different materials were chosen and simulated with CENOS.

Simulation results

	µ Workpiece	µ Concentrator	Position 1	Pos 2	Pos 3	Pos 4	Inductor-voltage [V]	Power [kW]
Original			**34,2**	**9,8**	**1**	**4,1**	**82**	**40,2**
V4_100_200	100	200	34,95	9,4	0,65	3,8	86,4	45
V4_100_1000	100	1000	34,87	9,55	0,58	3,87	87,2	45,1
V4_200_1000	200	1000	34,62	9,89	0,49	4	94,8	54,7

Comparison of different calculations with different permeabilities of the magnetic concentrator and the workpiece

	µ Workpiece	µ Concentrator	Position 1	Pos 2	Pos 3	Pos 4	Inductor-voltage [V]	Power [kW]
Original			**34,2**	**9,8**	**1**	**4,1**	**82**	**40,2**
V4_100_200	100	200	2,2%	4,1%	35%	7,3%	5%	12%
V4_100_1000	**100**	**1000**	**2,0%**	**2,6%**	**42%**	**5,6%**	**6%**	**12%**
V4_200_1000	200	1000	1,2%	0,9%	51%	2,4%	16%	36%

The best result was achieved with the following values:

- µ_workpiece = 100
- µ_concentrator = 1000

Optical match

- The isoline of 825 °C is shown in black and is the transition point for the change in the structure
- The hardness zone of the simulation visually matches the laboratory test
- μ workpiece = 100, μ electrical sheets = 1000

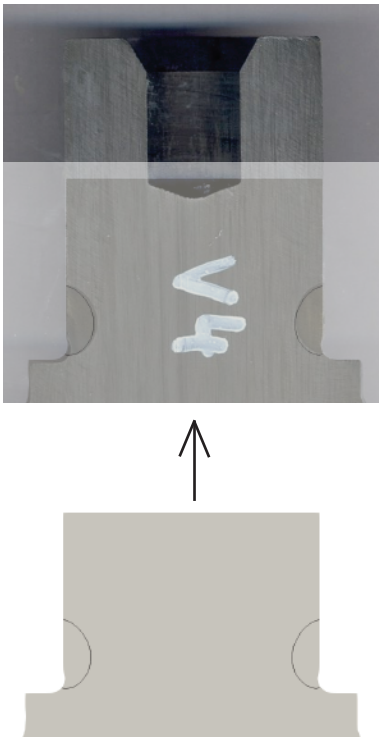

Conclusion:

With the help of CENOS, SMS Elotherm engineers can reliably experiment with different parameters and draw conclusions before physical prototyping.

Actual results accurately match the 3D simulation when observed visually.

CENOS Validation Cases

We will demonstrate cases of induction heating of a billet performed on CENOS simulation software. The results of the simulation are compared with experimental works 1) by Scurtu & Turewicz at Leibniz University of Hanover [2] and 2) Di Luozzo et al. at University of Buenos Aires [3].

Mathematical model in general

Magnetic vector potential A and electric scalar potential V formulation is used (AV-formulation):

$$\nabla \times (\nu \nabla \times \vec{A}) - \nabla(\nu \nabla \vec{A}) + \sigma\left(\frac{\partial \vec{A}}{\partial t} + \nabla V\right) = 0, \ in\ \Omega_1;$$
$$\nabla \times (\nu \nabla \times \vec{A}) - \nabla(\nu \nabla \vec{A}) = J_s, \quad in\ \Omega_2;$$

$$-\nabla\left(\sigma \frac{\partial \vec{A}}{\partial t} + \sigma \nabla V\right) = 0, \quad in\ \Omega_1.$$

Here, ν=1/μ - reluctivity, μ - permeability, σ – electrical conductivity, J_s – source current density. Ω_1 stands for a electrically conducting eddy current domain (a workpiece to be heated), Ω_2 stands for a non-conducting domain (air) and a domain with a current source (a coil).

Magnetic vector potential at an outer surface of a computational domain is equal to 0:

$$\vec{A} = 0.$$

For a symmetry axis of an axial symmetric model, the flux-parallel boundary condition is used:

$$n \times \vec{A} = 0.$$

For a symmetry plane, which is used to cut a half of the geometry in respect to the mirror-symmetry (in 2D representation, the plane is reduced to the line), the flux-normal condition is defined:

$$n \cdot \vec{A} = 0.$$

Temperature field is determined by solving the heat transfer equation:

$$\rho(\mathrm{T}) c_p(T) \frac{\partial T}{\partial t} = \nabla(\lambda(T) \nabla T) + Q.$$

Here, ρ – density, c_p – specific heat capacity, λ – thermal conductivity, Q – Joule heat source. On the outer surface of the tube, both convective and radiation heat losses are set:

$$q = h(T - T_{amb}) + \sigma_B \varepsilon (T^4 - T_{amb}^4).$$

Here, σ_B – Stefan Boltzmann constant, h – heat transfer coefficient, ε – emissivity.

Magnetic field changes over the period of harmonic oscillations. Therefore, for the harmonic calculation, specific integration procedure should be introduced to describe non-linear magnetic properties in harmonic equation correctly. According to that, magnetic field intensity varies over the period in ferromagnetic material not as sinusoidal function, but linearization approach finds effective B_{eff} that leads to same integral energy as it would be in transient simulation [4]:

$$B_{eff}(H) = \frac{2}{H} \int_0^H B(H') dH'.$$

The mathematical model described in this section is solved numerically with the Finite Element Method (FEM), coded in open source tool GetDP. For time-efficiency, CENOS platform was used to set material and numerical parameters of the model in graphic mode as well as to combine GetDP computational algorithms with pre-processing tool Salome and post-processing tool ParaView.

Description of the validation cases

Validation of numerical models were performed using 3 different cases, each of the case stands for the respective experimental results (the references are provided):

Case 1.1 – linear model for aluminum, ref. [2];
Case 1.2 – μ(T) model for carbon steel, ref. [2];
Case 2.0 – B(H,T) model for carbon steel, ref. [3].

In the Case 2.0, the full non-linear magnetic model is represented by magnetic permeability as a function of both magnetic field intensity and temperature – μ(H,T):

$$\mu(H,T) = \frac{B(H)}{H}\left(1 - \left(\frac{T}{T_C}\right)^{\alpha}\right) + \mu_0, \qquad (1)$$

where T_C is the Curie temperature, α is characteristic exponent of permeability temperature dependence and μ_0 is vacuum magnetic permeability. In the Case 2.0, α = 6; the Curie temperature T_C=735 °C.

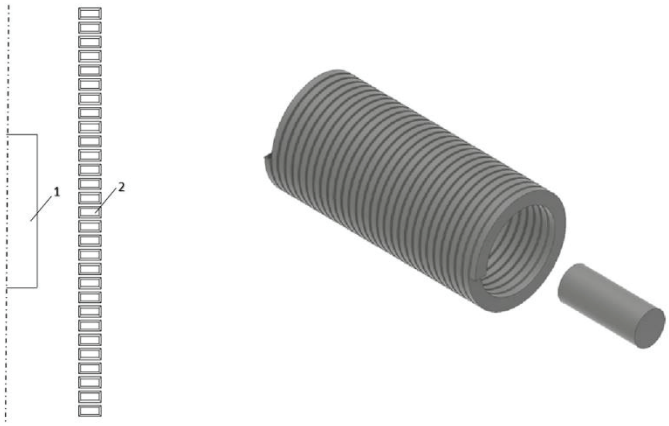

*Figure 1 – **Case 1.1 & 1.2**: 3D rendering of the parts (right) and the scheme of 2D axially symmetric system (left). On the scheme: 1 – the billet, 2 – the coil.*

*Figure 2 – **Case 2.0**: 3D rendering of the tube and the coil (right) and the scheme of 2D axially symmetric system (left). On the scheme: 1 – the tube, 2 – the coil.*

Table 1 – Case 1: Parameters of the validation cases

	Case 1.1	**Case 1.2**	**Case 2.0**
Geometric parameters			
Radius of the billet	30 mm		Inner: 16.5 mm/ Outer:
Length of the billet	150 mm		150 mm
Inner radius of the coil	70 mm		35 mm
Length of the coil	400 mm		50 mm
Number of windings	29		4
Operational parameters			
Current	1.3 kA	1.3 kA	725 A
Frequency	1.9 kHz	1.9 kHz	15 kHz
Material properties			
Material	aluminum	steel	
Thermal conductivity	λ(T), see Fig.3	λ(T), see Fig.4	
Heat capacity	c_p(T), see Fig.3	c_p(T), see Fig.4	
Density	2.45 g/cm^3	7870 g/cm^3	
Electric conductivity	σ(T), see Fig.3	σ(T), see Fig.4	
Magnetic properties			
Over temperature	**constant μ = 1**	**μ(T)**, see Fig.5	**B(H,T)**, see Eq.(1)
B-H curve	-	-	**B(H,T)**, see Fig.6

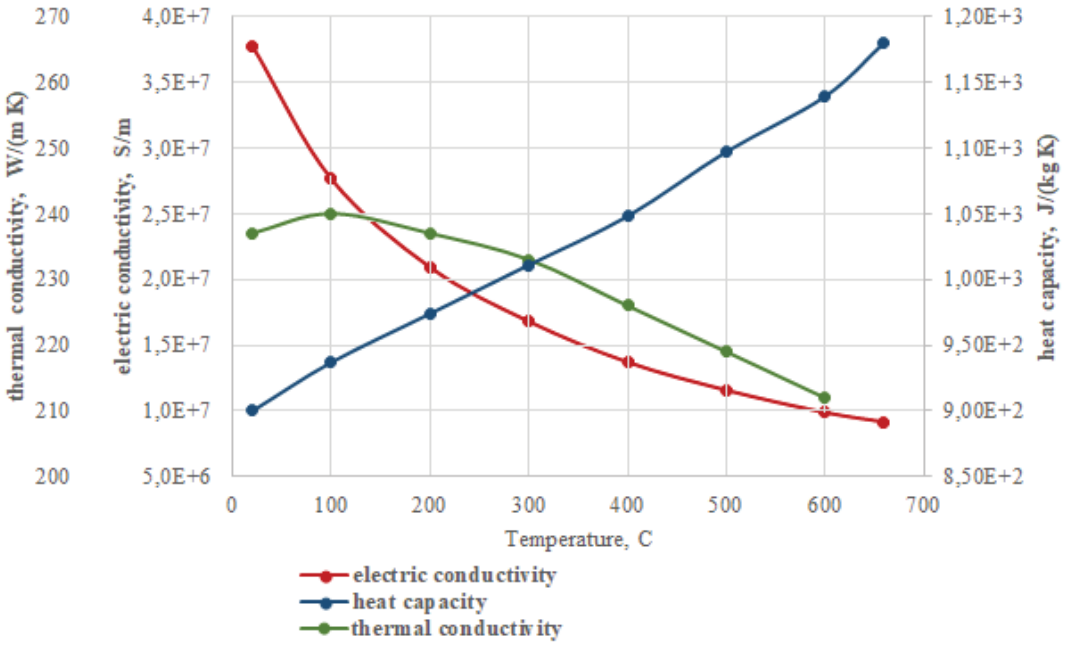

*Figure 3 – **Case 1.1**: temperature dependent material properties of **aluminum**.*

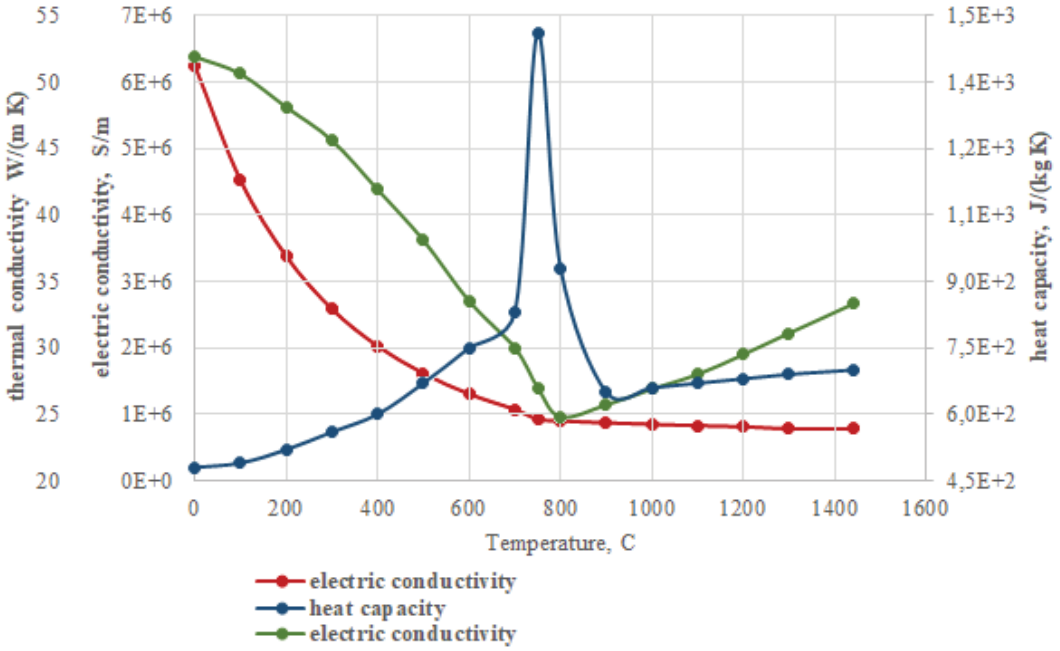

*Figure 4 – **Case 1.2 & 2.0**: temperature dependent material properties of **steel**.*

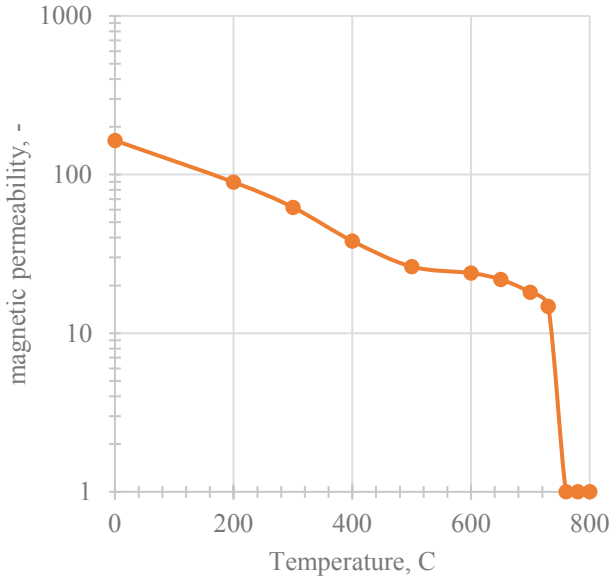

*Figure 5 – Case 1.2: Magnetic permeability of steel μ **over temperature.***

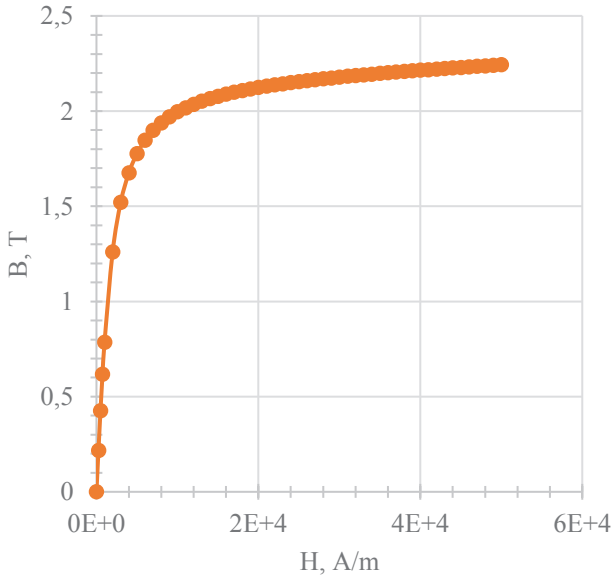

*Figure 6 – Case 2.0: **B-H curve***

Case 1.1: Linear model for aluminum

Case 1.1 represents the simple linear model for induction heating of the aluminum billet. Fig.7 demonstrates that the results, obtained using the open source software GetDP, perfectly match both results of benchmark simulation by ANSYS and the experimental results [2]. The results represents temperature in the middle of the billet, at the symmetry axis, over heating time.

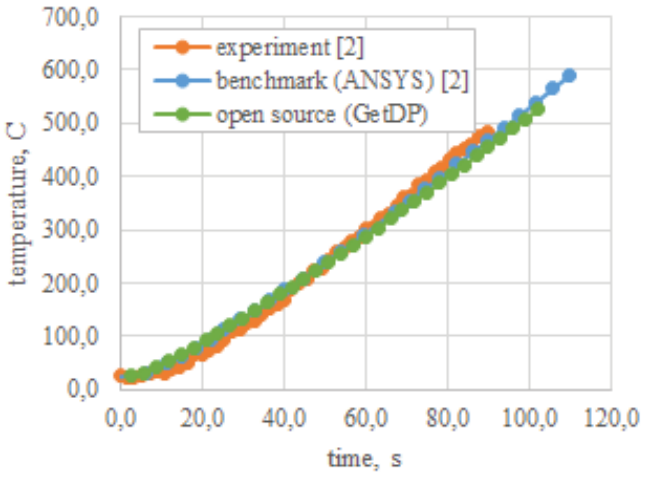

*Figure 7 – **Case 1.1**: Temperature at the middle of the aluminum billet over heating time. Experimental results and benchmark calculation ref. [2].*

Case 1.2: μ(T) model for steel

It is transparent, that induction heating simulation of steel requires to consider non-linear properties of ferromagnetic materials. Frequently, simulation is limited to temperature dependence of magnetic properties μ(T) and does not take into account a B-H curve. Such approach is demonstrated also in the article [2], which presents the experimental results of induction heating of a steel billet obtained by Scurtu & Turewicz at Leibniz University of Hanover. Beside the experimental results, the authors published numerical results by ANSYS Classic, which is well-known accurate benchmark software (see Fig.8). While the simulation by Scurtu & Turewicz is performed taking into account only temperature-dependence of magnetic permeability μ(T), the simulated temperature perfectly matched the asymptotic (steady state) value, however, significantly underestimates temperature during transient heating. E.g., at 10th second, the benchmark model of ANSYS predicts the surface temperature of the steel billet 100 °C less than measured during the experiment.

The simulation by open source tool GetDP coincides with the benchmark simulation, even more, slightly better predicts transient temperature during heating (see Fig. 8). The last fact is just because of adaptive time step, which allowed more accurately resolve the temperature raise. Nevertheless, the figure clearly demonstrates inability of the simple μ(T) model to predict temperature at the surface of the steel billet during the heating process.

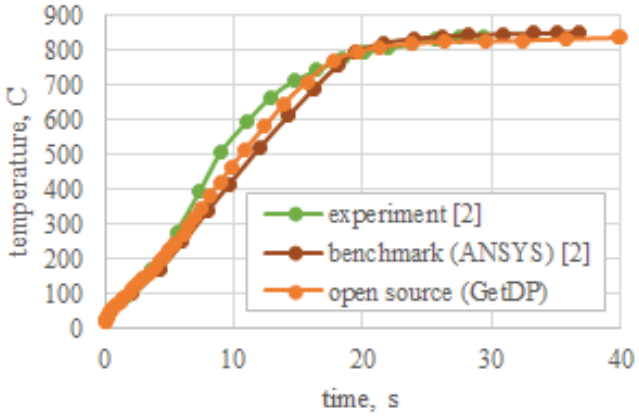

*Figure 8 – **Case 1.2**: Temperature at the surface of the steel billet over heating time. Experimental results and benchmark calculation of **μ(T) model** ref. [2].*

Does a B-H curve help to predict the temperature raise accurately? While there is no exact information available neither regarding the grade of the steel used in the experiment, nor B-H properties of it, the simple calibration of some analytical B-H model demonstrates improvement of simulation result on Fig. 9. However, one can recognize slightly overestimated temperature after 10th second of heating. Since B-H curve here is just calibrated and does not ground in material properties of the steel, we decided to double check necessity of the B(H,T) model in the Case 2.0, which provides very accurate experimental data.

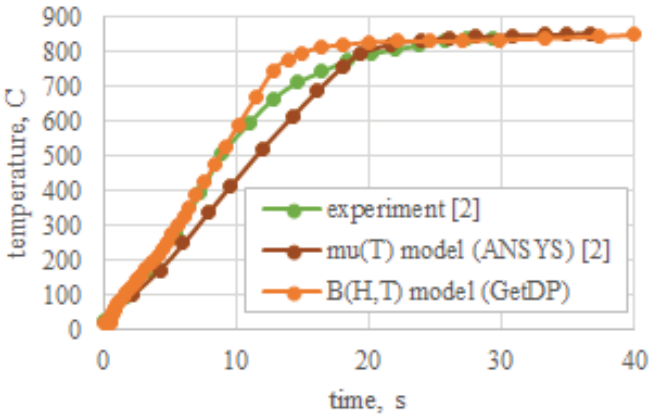

*Figure 9 – **Case 1.2**: Temperature at the surface of the steel billet over heating time. Calibrated **B(H,T) model** and μ(T) model (ref. [2]) benchmarked to experimental results [2].*

Case 2.0: B(H,T) model validation

The Case 2.0 demonstrates accurate validation of B(H,T) model in respect to experimental data obtained by Di Luozzo et al. at the University of Buenos Aires [3]. The non-linear model is represented by Eq.(1) and Fig.6. Fig.10 demonstrates numerical mesh created for the following simulation.

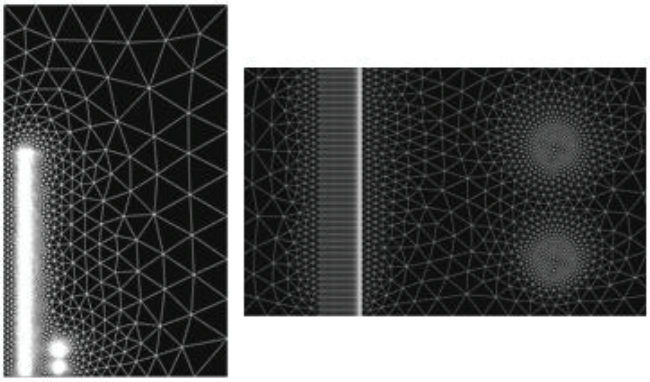

Figure 10 – Case 2.0: Model mesh

While Fig.11 demonstrates simulated temperature distribution at the surface of the billet, Fig.12 presents the essential results, comparing temperature over time at the surface of the billet. Temperature maxima is located in the coil region and it falls rapidly outside of coil where no heating source is present. The curves represent the points at different distance from the plane or mirror-symmetry of the system.

Fig.12 demonstrates good match of simulation results with the accurate experiment.

Discussion of the results

In general, good agreement between numerical and experimental results is achieved. Main discrepancies are as follows:

- change in heating rate at the symmetry plane appears 2 seconds earlier in numerical results rather than according to the experimental data. It might be because of the fact, constant voltage regime was carried out at the experiment, while only constant current regime in possible to simulate in 2D approximation. So, while the current in the simulation model was constant during all simulation time, it was, obviously, increasing during the initial short time moment in the experiment;
- change in the heating rate at the symmetry plane appears at lower temperatures ($\Delta T \approx 15$ K) in simulation results than in experimental results. We would like to argue here that the precise Curie point for the steel used is not known. Simulations at different Curie temperatures show that this change always appears slightly above (10-15 K) Curie point (see Fig.13 and further discussion).

Change in heating rate appear at 747 °C, which is 10 degrees higher than Curie point. The same character is observed in simulations for variation of Curie temperature (see Fig.13). Furthermore, increased heating rate appears immediately after Curie point for short period. This might be explained with electromagnetic effect of joined materials [5], which leads to local Joule heat maxima in non-magnetic part of steel above Curie point.

Fig. 13 demonstrates sensitivity of the B(H,T) model to Curie temperature. While for many steel grades is not known, variation of T_C might lead to slightly different results in heating simulation.

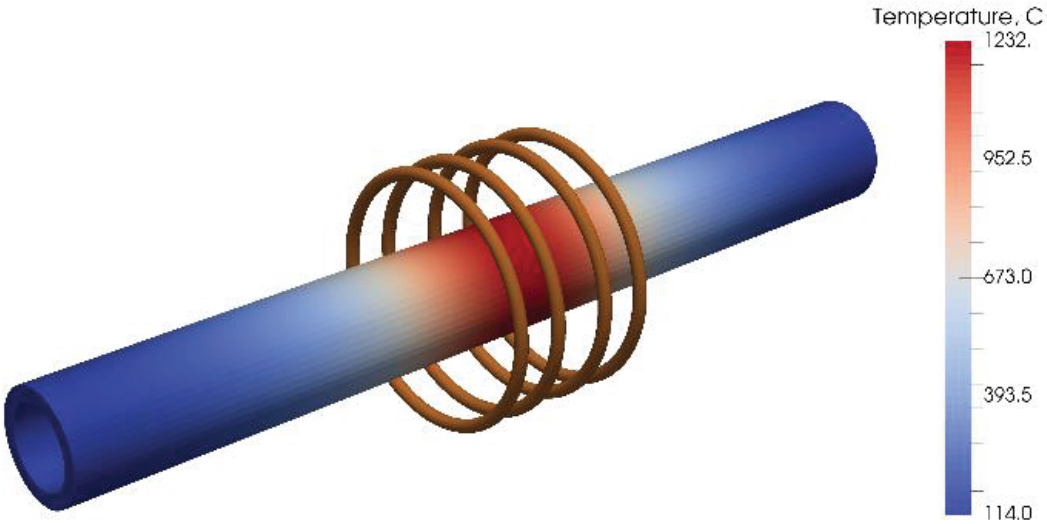

Figure 11 - Case 2.0: Temperature distribution in the tube after 120 seconds

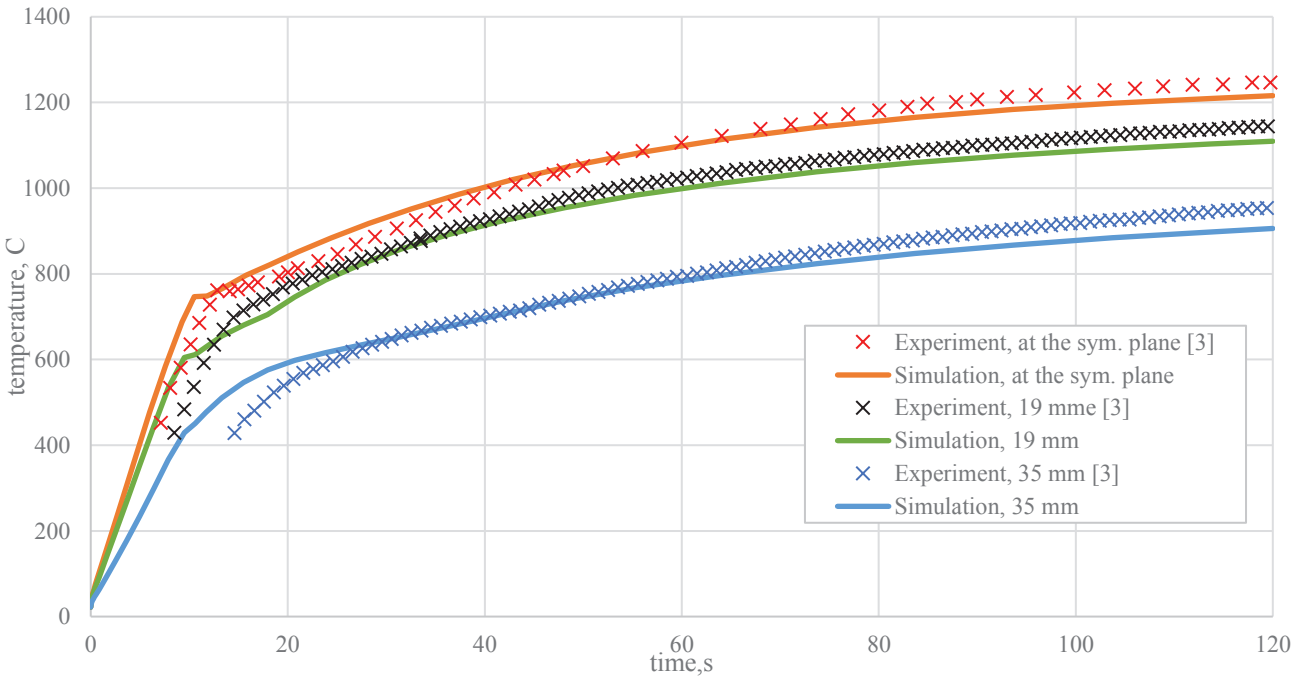

*Figure 12 – **Case 2.0**: Simulation and experimental results (ref. [3]) of temperature at the surface of the steel billet. The curves differs with the point where the temperature was measured, the distance from the symmetry plane is specified in the legend.*

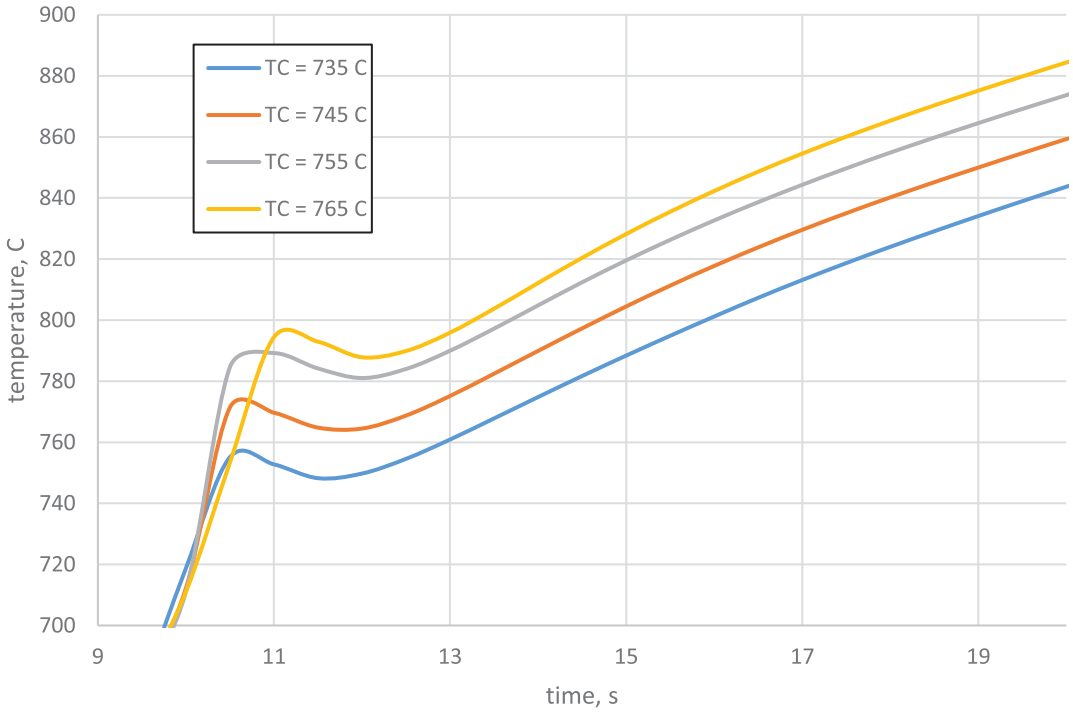

*Figure 13 – **Case 2.0**: Variation of Curie temperature in the B(H,T) model (Eq.1).*

Conclusion

Open source software GetDP has proven to be very reliable for modeling induction heating applications, especially due to its capability to capture temperature dependent material properties and non-linear magnetic effects. Results obtained with GetDP are in good agreement both with ANSYS commercial software and experimental results.

Simulation of non-magnetic materials or the materials with linear magnetic properties is easy to perform with the highest level of accuracy, since mathematic model is relatively simple. The results shown in the paper demonstrated perfect match with the experimental results.

Nevertheless, simulation of such ferromagnetic materials as steel request more accurate description of non-linear magnetic properties. Although, temperature dependent magnetic permeability $\mu(T)$ leads to satisfactory prediction of asymptotic (steady state) temperature, it might significantly underestimate temperature at the surface of soft magnetic materials like steel while heating. Then, the full non-linear model, which includes $B(H,T)$, leads to accurate prediction of temperature, which was validated by experimental results.

We would like to point out that turning from the linear model to the full non-linear model for ferromagnetic materials, results of simulations become very sensitive to material property data. While in many practical cases, there might be insufficient knowledge of exact material properties, it might be reason for non-accurate prediction of heating pattern. As the example, slightly variation of the Curie point, which depends on steel grade, was simulated in the paper, which led to variation in heating pattern of the billet.

At the end, we would like to point out the value of CENOS platform, which enabled for the authors of the paper time-efficient simulation of induction heating problems using open source algorithms of GetDP software. CENOS turned out into the simple, fast and accurate way to perform heating simulation.

References

[1] ASM Handbook, Volume 4C: Induction Heating and Heat Treatment, ed. By Rudnev, V. & Totten, G. E., ASM International (Materials Park, OH, 2014).

[2] Scurtu, G. L. & Turewicz, P., "Numerical Modeling of Static Induction Heating," *Proc Engineering Numerical Modeling and Simulation*, Sinaia, Romania, September 2012.

[3] Di Luozzo, N., Fontana, M., Arcondo, B., "Modelling of Induction Heating of Carbon Steel Tubes: Mathematical Analysis, Numerical Simulation and Validation," *Journal of Alloys and Compounds*, Vol. 536S (2012), pp. S564-S568.

[4] Paoli, G., Biro, O., Buchgraber, G., „Complex representation in nonlinear time harmonic eddy current problems," *Magnetics, IEEE Transactions*, no. 34, pp. 2625 - 2628. 10.1109/20.717607.

[5] Rudnev, V., Loveless, D., Cook, R., Handbook of Induction Heating, Second Edition, CRC Press (Boka Raton, 2018).

Acknowledgement

L. Scurtu and N. Di Luozzo are gratefully acknowledged for providing detailed data of their experiments (referenced in the paper) and some clarifying discussions.

3. Return On Investment Case Studies

3.1. Production plants - induction heating equipment end-users

ThyssenKrupp Presta Schönebeck - saved 90% on tooling and 30% on energy

Marcus Hellriegel – an engineer at ThyssenKrupp Presta in Schönebeck (Elbe) near Magdeburg in Germany, managed to design a new induction coil for hardening of the ball track inside a ball nut (a steering system part) which reduced the tooling costs per part by 90% and energy consumed by 30%, which resulted in seven-digit savings for the company per year. Marcus was able to complete the new design just in a couple of months in a very cost-efficient way by using CENOS Induction Heating simulation software and 3D-printing technology.

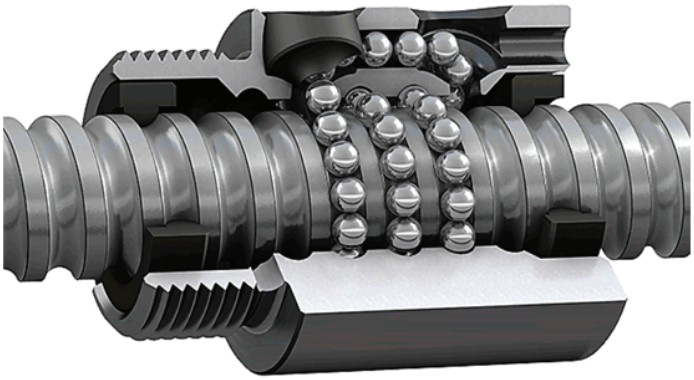

The inner ball track

The problem Marcus was trying to solve was a very short lifetime of the so-called hairpin-type coil used for hardening of the inner ball track. Thus, Marcus' primary goal was to improve the coil design to achieve a longer lifetime and lower production costs. It took about 10 design iterations to come up with the new coil shape, which demonstrated excellent results in tests. Now, ThyssenKrupp is pending the patent for this brand new coil design. For this job, Marcus decided to use simulation software to test design candidates virtually and 3D print the final coil. Here are the economics behind this decision:

	Production time with delivery	The approximate cost (with Fluxtrol material)
Conventionally manufactured coil by a supplier	4-5 working days	EUR 6,000
3D-printed coil by a supplier	2-3 working days	EUR 1,000
3D-printed coil inhouse	within a day	EUR 800

Thus, if things were done the traditional way by ordering conventionally manufactured coils from a supplier, 10 design & prototyping iterations would take more than a half-year (taking into account the time for design, tests and result analysis) and would cost around EUR 60,000 just for different coil design version trials. For such a sophisticated coil type, one could save time by ordering 3D printed coil prototypes from an additive manufacturing supplier but still it would take 3-4 months and cost around EUR 10,000.

Marcus decided to learn the simulation software to be able doing all design iterations by means of the computer simulation and 3D-print the final design candidate for the real-life test. From all simulation software available in the market, Marcus chose CENOS because it is focused on induction heating and ensures unmatched speed of learning due to its straight-to-the-point interface for induction tasks. So, the new design of the coil was completed in a couple of months. The use of simulation unleashed the engineering talent of the designer allowing to test even the craziest ideas at no extra cost – everything was tested virtually on a PC and eventually fabricated with the help of 3D printing.

When the new coil was 3D-printed, it was time for the lab tests. It was surprising that the test demonstrated up to 30% of energy saving for the newly-designed coil compared to the old one. The reason for this dramatic increase of energy efficiency is due to the fact that the 3D-printed coil has no soldering joints. This particular inductor type, if conventionally manufactured, has up to 20 soldering joints – each joint increases overall coil resistance that results in a higher energy consumption. A 3D-printed coil on the contrary has zero solderings – thus, lower electric resistance.

While the main goal of the project was to create a new design for the coil that will not break so often, tremendous savings came from lowered production costs and increased energy efficiency of the coil. The coil efficiency was enabled by 3D-printing technology, and simulation software made the design process extremely efficient. That all, multiplied by the engineering talent of Marcus Hellriegel, led to an exceptional return on investment (ROI) for the combination of CENOS simulation software (EUR 7,800 per year) and the 3D-printed part (EUR 1,000 per coil) which resulted in saving 90% on tooling and 30% on energy costs.

GKN Driveline Celaya - increased overall equipment efficiency (OEE) for a CV joint hardening line by 9%

Kevin Tovar Estrada - a manufacturing engineer at GKN Driveline Celaya in Mexico, supervises induction hardening lines at the plant. He created a hardening "cookbook" – an algorithmic instruction for a machine operator to troubleshoot wrong hardening results. For example, the operator can change the gap size between a part and an inductor to correct the hardening profile when there is a slight change in part design, or some other parameters changes – quenching liquid, outside temperature, steel, etc. The operator makes an inspection of the hardening profile by cutting the part. If there is a deviation from the desired profile, he/she adjusts the parameters according to the "cookbook", which ensures a reliable result with less scrap.

Simulation software helped Kevin to create such a cookbook 60% faster than in the traditional way with physical experiments. For a CV joint shaft hardening, the simulation approach also saved about 14 parts, which would be otherwise wasted. As a result, the production process runs with 60% less scrap.

Kevin did comparison tests to choose the right simulation software. CENOS - an induction heating specialized simulation software, demonstrated exceptionally good results: case preparation (setting of geometry and operational parameters) was 10 times faster than with other software, while calculation time was the same or faster. There was also a handy function that simplified the model by using constant magnetic permeability for faster calculation – the feature which was absent in other software. Total time for simulation analysis of a CV joint shaft hardening took 7.5 hours with CENOS.

To be sure about the results, Kevin compared the simulated hardening profile with the cross-section cut of the real part, the software had prediction accuracy of 93.8%. Then, Kevin redesigned the coil for CV joint hardening based on the simulation. He altered the position of flux concentrators and found a better design which eliminated local overheating. Old coil design failed and started leaking after 20,000 shots, while the redesigned coil is still running after 122,000 shots – more than five-fold improvement of the coil lifetime.

By summing all of the benefits of the simulation software adoption in the engineering routine of the plant, Kevin got a 9% increase of the overall equipment efficiency (OEE).

Netzsch do Brasil reverse engineered hidden operational parameters of their induction machines for R&D

Klaus Heizinger - the head of research and development at hydraulic pump producer Netzsch do Brasil, is responsible for the production process R&D, efficient hardening of parts is an important part of his work. The company purchased an induction hardening machine a couple of years ago. Multiple things had changed since then - the design of the parts, the steel used, etc., as Netzsch was constantly working to improve their products and manufacturing processes. When trying to adjust the hardening process, Klaus and his colleagues were struggling to get satisfactory results. The main reason was very limited control over the hardening machine. "The operational interface gave us almost no quantitative data of the process", explained Klaus. "For example, there are just three options for the frequency: high frequency, medium frequency, and low frequency, without any information of what are the absolute values of those frequencies. So, the engineers were wasting parts and time by doing numerous experiments, but still were struggling to get good results in many cases" Klaus admitted. Then, Klaus decided to purchase a specialized induction heating simulation software with an idea to support reverse engineering of the machine settings for a better understanding of the process. That turned out to be a successful approach. "Now, we know much better what and how our machine can do", proudly reported Klaus, "thus, we can work on the process improvements with confidence, experiment with new materials for parts. CENOS significantly improves R&D at our plants."

Volkswagen Group Services achieves fivefold productivity increase of power steering rack mounting production

Marcel Ruthmann - a young engineer at Volkswagen Group Services in Braunschweig, Germany, began using simulation to increase the efficiency of induction heating in the production processes of the company. While the majority of his successful projects will remain hidden for external observers, there is one worth a mention. By means of simulation with CENOS software and working together with Fabian Bauer - an engineer at Volkswagen in Wolfsburg, Marcel reduced the induction heating time for the mounting of the power steering rack about 5 times - from 9 seconds down to 2 seconds. Thus, the productivity of power steering parts manufacturing line is almost 5 times higher now.

3.2. Induction heating equipment manufacturers and service providers

GH Induction saved 50% on the design and manufacturing time of induction coils for their customers

Juan Carlos Rodriguez Lara - an application and process manager at GH Electrotermia, the headquarter of GH Induction Group in Valencia, Spain, oversees the development of customer projects like induction coil design. The company provides a unique service offering the design and 3D printing of inductors (3Dinductors.com) utilizing electron beam melting (EBM) technology. Combining this technology with CENOS simulation GH shortened the time to discover and demonstrate coil design improvements to their customers and currently provides the utmost reliability and maximum performance of the inductors.

With one of the latest cases, Juan Carlos' engineers managed to achieve 50% savings on the design and production time which led to surprising their customer with exceptionally fast delivery of a top-quality inductor. The customer's request was to redesign the coil to meet the change in the hardening profile specification for wheel hub production the customer did. So, GH Electrotermia needed to adapt the inductor design quickly to meet the new requirements.

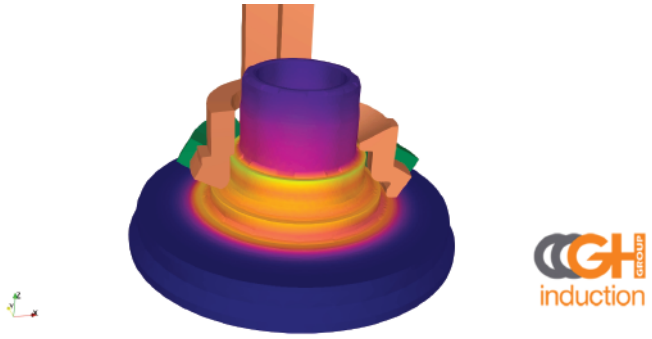

Inductor prototype simulation before 3D printing

First, the heating pattern was simulated for the customer's original inductor design. Based on induction heating experience it was pretty clear which parameters had to be modified in the coil to meet the new specifications. A couple of simulations later the design was nailed - way faster than producing prototype inductors and testing them in a lab. Since GH's 3D printing technology allows absolute freedom of external and internal design (cooling improvement, hot spot elimination, section strength, etc.), the new better design was proposed by the engineering team of GH and fulfilled by 3D printing in a few hours.

SMS Elotherm gets desired hardening profiles with the first inductor design built

Judith Levermann - a process development engineer at SMS Elotherm in Remscheid, Germany, is responsible for the design of inductors and hardening processes for sophisticated customer cases. "With CENOS, we are able to develop inductors for new hardening cases without large expenses and set up more advanced heat treatment approaches without multiple lab trials," Judith explained.

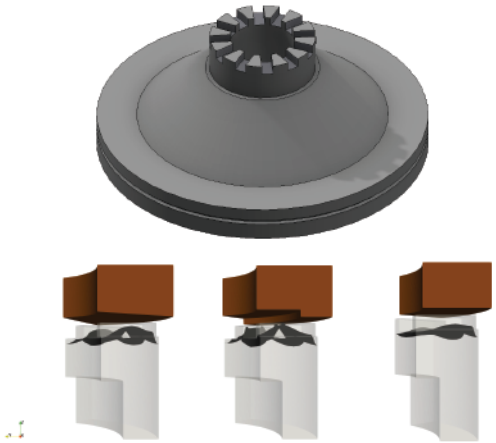

Ring inductor for a gear ring

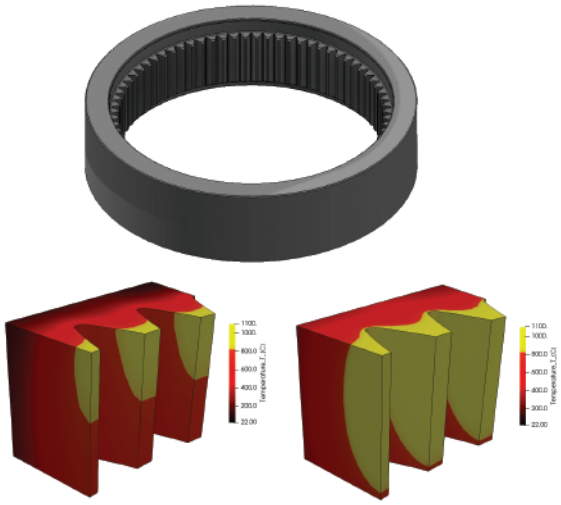

Hardening of a gear with scanning inductor

Judith agreed to share two examples of the design she performed: ring inductor for a gear ring (the upper image) and pre-heating followed by hardening of another gear with scanning inductor (the lower image). "We had many ideas on how to harden the tooth area of the gear ring. However, we wanted to try out different options without creating large expenses but also meet the hardening zone requirements with the first inductor built," Judith explained the motivation behind the use of simulation. Without any experiments and in a very short time, the process department was able to test all ideas and selected the best performing one. When the inductor was built, Judith ran the physical test and found the zone affected by hardening matched well with the predicted zone by the 3D model in CENOS.

3.3. German Mittelstand (small companies) for induction heating design and tooling

The last two stories are from small German companies, so-called Mittelstand, which work as induction heating tooling shops and hold a huge number of orders from the automotive industry due to decades of experience they have in the engineering of induction projects. The induction-heating-specialized simulation software CENOS helps them by supporting their experience with bullet-proof evidence that attracts more orders and demonstrates sustainably good results even upon the change of engineer's generations.

"We are a small induction heating company with more than 30 years of experience in designing excellent induction systems," told Cay-Oliver Bartsch - the owner & director of COBES in Ettenheim, north from Freiburg. "Nevertheless, when we approach new customers, they still want to be 100% confident in our work. Simulation helps us to visualize results, ensure customers, and eliminate friction in getting orders."

"Already in the first month of using CENOS, we have been able to close several coil design projects," proudly told Lucas Tebes - an engineer at Lötec in Rheinmünster south from Karlsruhe, the son of the founder of the company Harald Dieter Tebes. "The results of the simulation have been spot on and fully match real-life cases. CENOS has helped us a great deal," Lucas adds.

From cost and time savings in tooling and process design to less friction in customer acquisition - these are the benefits of the fourth industrial revolution, provided by computer aided engineering which is becoming more and more accessible and affordable for small and medium-sized companies and engineers with no previous simulation experience.

4. CENOS Tech Stack

4.1. Workflow and third-party open-source tools

- **Geometry: Templates (CENOS)**
  From CAD (CENOS)
  Editor (Salome)
- **Physics (CENOS)**
- **Results: 3D/2D visualization (Paraview)**
  Spreadsheet (CENOS)

4.2. Algorithms

FEM - first order, A-V formulation, frequency domain and transient; stationary and non-stationary heat transfer equation with Joule heat source

1 Electromagnetic induction

High frequency electric and magnetic fields are always present in induction heating applications. Any electromagnetic process is described by Maxwell equations, which are simplified for the condi tions used in technological applications. In the IH system description, the charge accumulation can be neglected since all conducting parts are usually grounded. The displacement currents can be neglected as well because of sub-GHz frequency range used in such applications. Both mentioned simplifications lead to the so-called quasi-stationary approximation:

$$\nabla \cdot \vec{E} = 0 \tag{1.1}$$

$$\nabla \cdot \vec{B} = 0 \tag{1.2}$$

$$\nabla \times \vec{E} = -\frac{\partial \vec{B}}{\partial t} \tag{1.3}$$

$$\nabla \times \vec{B} = -\mu_0 \vec{j} \tag{1.4}$$

Here, E is electric field intensity, B is magnetic flux density, j is current density, t is time, and μ0 is magnetic permeability of free space. Combination with Ohm's law (equation 1.5) and insertion of equation 1.3 in 1.4 leads to the equation system that can be solved to describe induction processes.

$$\vec{j} = \sigma[\vec{E}] \tag{1.5}$$

$$\frac{\partial \vec{B}}{\partial t} = \frac{1}{\mu_0 \sigma} \nabla^2 \vec{B} \tag{1.6}$$

$$\nabla \vec{j} = 0 \tag{1.7}$$

where σ is electrical conductivity. For more convenient solution of equations 1.5-1.7, potentials are usually introduced – magnetic vector potential A and electric scalar potential Φ that are defined as follows:

$$\vec{E} = -\nabla \Phi - \frac{\partial \vec{A}}{\partial t} \tag{1.8}$$

$$\vec{B} = \nabla \times \vec{A} \tag{1.9}$$

For the solution of AC current systems, further simplifications are used. Since the source current can be written as I = I0exp(ωt), the magnetic field (and vector potential) can be expressed in the same way B = B0exp(ωt). ω = 2πf is angular frequency, where f is field oscillation frequency. Eq. 1.6 written for vector potential becomes the following form

$$\omega \vec{A} = \vec{u} \times \nabla \times \vec{A} + \frac{1}{\mu_0 \sigma} \nabla^2 \vec{A} \tag{1.10}$$

For the uniform external magnetic field in an infinite conductor half–space,complex magnetic field distribution is expressed as follows:

$$B = B_0 exp\left[-\frac{x}{\delta}\right]\left[cos\frac{x}{\delta} - sin\frac{x}{\delta}\right] \tag{1.11}$$

$$\delta = \sqrt{\frac{1}{\sigma \mu \pi f}} \tag{1.12}$$

Eq. 1.12 describes the skin layer depth for magnetic field – the distance in which magnetic field decays e times. Induced currents generate heat in the melt that is also able to influence the fluid motion by creating a nonuniform temperature distribution. The induced Joule heat is expressed as:

$$Q = \frac{\vec{j}^2}{\sigma} \tag{1.13}$$

In time-harmonic analysis, Joule heat density can be calculated by time averaging over one period of electromagnetic field oscillation.

$$Q = \frac{\vec{j}_0^2}{2\sigma} = \frac{\vec{j}_{Re,0}^2 + \vec{j}_{Im,0}^2}{2\sigma} \tag{1.14}$$

Here subscript 0 represents complex amplitude. The skin depth of the electromagnetic field is not the universal parameter for the characterization of the EM field impact depth. The relation of δ with size of the domain is also significant. For this purpose, dimensionless frequency ω is introduced as follows

$$\tilde{\omega} = \omega\mu_0\sigma L^2 = 2\left(\frac{L}{\delta}\right)^2 \tag{1.15}$$

In literature, the dimensionless frequency is also widely called as shielding parameter or shielding factor.

2 A-Φ weak formulation

The A-Φ formulation uses magnetic vector potential A both in Ω1 - eddy current region and Ω2 - free space, and an additional electric scalar potential Φ in Ω1. The fields obtained from the potentials can be computed from Eq 1.8 and 1.9. The Maxwell equations for time-varying fields written in potential form are

$$\nabla \times \frac{1}{\mu} \times \vec{A} + j\omega\sigma\vec{A} + \sigma\nabla\Phi = 0 \tag{2.1}$$

$$\nabla \cdot (j\omega\sigma\vec{A} + \sigma\nabla\Phi) = 0 \tag{2.2}$$

$$\nabla \times \frac{1}{\mu}\nabla \times \vec{A} = \vec{J}_s \tag{2.3}$$

where μ - permeability, σ - conductivity of the media. The numerical approximation of the potentials is performed using a finite element mesh. The potentials are expressed in terms of shape functions associated with the nodes of this mesh as

$$\vec{A} = \sum_{j=1}^{n}(A_{xj}N_j\hat{x} + A_{yj}N_j\hat{y} + A_{zj}N_j\hat{z} \tag{2.4}$$

$$\Phi = \sum_{j=1}^{n}\Phi_j N_j \tag{2.5}$$

where Axj , Ayj , Azj and Φj are the three Cartesian components of the vector potential and the scalar potential at nodes j ; and Nj is the shape function associated with node j that assumes the value of one at this node and the value of zero at any other node. The vectors ˆx, y, ˆ zˆ are the Cartesian unit vectors, and n is the number of nodes in the mesh.
Using Galerkin (weak) formulation, we obtain [2]

$$\int_{\Omega_1}(\frac{1}{\mu}\nabla\times\vec{N}_i)\cdot(\nabla\times\vec{A}) + \frac{1}{\mu}\nabla\cdot\vec{N}_i\nabla\cdot\vec{A} + j\omega\sigma\vec{N}_i\cdot\vec{A} + \sigma\vec{N}_i\cdot\nabla\Phi dV - \int_{\partial\Omega_1}\vec{N}_i\cdot(\frac{1}{\mu}\nabla\times\vec{A}\times n)dS - \int_{\partial\Omega_1}\vec{N}_i\cdot(n\frac{1}{\mu}\nabla\cdot\vec{A})dS = 0 \tag{2.6}$$

$$\int_{\Omega_1}(j\omega\sigma\nabla N_i\cdot\vec{A} + \sigma\ nabla N_i\cdot\nabla\Phi)dV + \int_{\partial\Omega_1}\sigma N_i(-j\omega\vec{A} - \nabla\Phi)\cdot ndS = 0 \tag{2.7}$$

$$\int_{\Omega_2}(\frac{1}{\mu}\nabla\times\vec{N}_i)\cdot(\nabla\times\vec{A}) + \frac{1}{\mu}\nabla\cdot\vec{N}_i\nabla\cdot\vec{A}dV - \int_{\partial\Omega_2}\vec{N}_i\cdot(\frac{1}{\mu}\nabla\times\vec{A}\times n)dS - \int_{\partial\Omega_2}\vec{N}_i\cdot n\frac{1}{\mu}\nabla\cdot\vec{A}dS = \int_{\Omega_2}\vec{N}_i\vec{J}_s dV \tag{2.8}$$

3 Electric Contact resistance BC

The steady-state equation of continuity of current density is

$$\nabla\vec{j}_c = 0 \tag{3.1}$$

where ~jc, is the conduction current density within the earth. Substituting Ohm's law (Eq 1.5).

$$-\nabla\cdot\sigma\nabla\Phi = 0 \tag{3.2}$$

Where there are sources of diverging current density (~js), ~jc is no longer divergenceless but equals the divergence of ~js. Eq. 3.1 becomes

$$-\nabla\cdot\sigma\nabla\Phi = \nabla\cdot\vec{j}_s \tag{3.3}$$

Equation 3.3, Poisson's equation, is the domain equation for the problem. For a point electrode at the origin, · ~js becomes I δ(x)δ(y)δ(z) where I is the current in the electrode and δ(x) is the Dirac delta function. The electrical boundary conditions for this problem are the continuity of the potential Φ and the continuity of the component of current ~jn normal to the boundary. The latter implies that σ(∂Φ ∂n), where n is the direction normal to the boundary, must be continuous. At the air-workpiece interface ∂Φ ∂n must be zero since σ is negligible in the air. [4]

4 Thermal contact resistance

To simulate thermal contact resistance, heat transfer coefficient must be known. Then on the surfaces of the domain, a convective heat flux boundary conditions have to be set

$$q = h(T - T_{amb}) \tag{4.1}$$

5 Surface impedance method

For magnetically linear materials, the surface impedance is defined using the classical definition of the skin depth δ

$$Z_{s,linear} = \frac{1}{\delta\sigma}(1 + j) \tag{5.1}$$

where σ is electric conductivity.
For magnetically nonlinear materials the definition of the surface impedance is based on the limit theory presented, e.g., Agarwal where a sinusoidal magnetic field $H = H_m\sin(\omega t)$ is assumed to be tangential to the ferromagnetic body. In the solution given by this limit theory the magnetic flux density has a constant value from the surface to a certain depth, i.e., Agarwal's skin depth δ_{ag} [1]

$$\delta_{ag} = \sqrt{\frac{H_m}{\sigma\pi f B_0(H_m)}} \tag{5.2}$$

where B_0 is the saturation magnetic flux density corresponding to the amplitude of the magnetic field H_m.
In most eddy current problems the magnetic field reaches the surface of the magnetic material in an almost normal direction. In these cases the electric field instead of the magnetic field, is assumed to be sinusoidal. Thus the surface impedance can be written [6]

$$Z_{s,non-linear} = \frac{27\pi^3}{2\sqrt{5}\sigma\delta_{ag}}\left(1 + \frac{4}{3\pi}j\right) \tag{5.3}$$

Equation 5.3 is valid only for high fields with strongly saturated materials. In low fields magnetic properties of material can be assumed to be linear, therefore equations 5.1 and 5.3 is combined together using weighted function $f(H_m)$ [3]

$$Z_s = f(H_m)Z_{s,linear} + (1 - f(H_m))Z_{s,non-linear} \tag{5.4}$$

where

$$f(H_m) = 2\left(1 - \frac{\int_0^{H_m}B(H)dH}{B(H_m)H_m}\right) \tag{5.5}$$

where B(H) corresponds to the real BH-curve of the heated material.[7] [8]

6 Stranded coil and Litz wire

Since geometrical discretization of every strand in the Litz wire requires high spatial resolution, it is useful to apply special models for Litz wires which allow simulating whole wire as a single solid domain. This requires correction factor for resistance. Several models are proposed, one of which is used in this work

$$r = r_{DC} F_R \tag{6.1}$$

d - wire diameter r- resistance per unit length, rDC - resistance per unit length for DC current, FR correction factor. The correction factor is represented in terms of Kelvin functions

$$F_R = \frac{\xi}{\sqrt{2}d}\left[\frac{K_{Ber}(0,\xi)K_{Bei}(1,\xi) - K_{Ber}(0,\xi)K_{er}(1,\xi)}{K_{Ber}(1,\xi)^2 + K_{Bei}(1,\xi)^2} - \frac{K_{Bei}(0,\xi)K_{Ber}(1,\xi) + K_{Bei}(0,\xi)K_{Bei}(1,\xi)}{K_{Ber}(1,\xi)^2 + K_{Bei}(1,\xi)^2}\right] \tag{6.2}$$

$$\xi = \frac{d}{\sqrt{2}\delta} \tag{6.3}$$

Here KBer and KBei are the real and imaginary parts of Kelvin function. When ξ is small, which corresponds to small frequency, the correction factor is 1 and the resistance is same as for DC. But from the value ξ = 2 the correction factor starts to grow. Consequently this correction factor influences the power in the coil.

7 Calculation of microstructure of ferrite + cementite phase

Regions where specific microstructure exist are mapped in TTT diagram 7.1 and can be used to calculate what kind of microstructure will be formed during cooling of a steel.

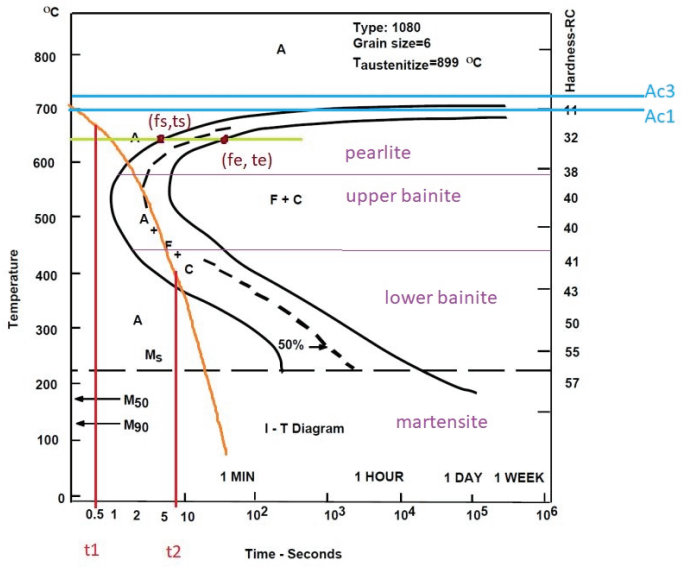

Figure 7.1: TTT diagram. A - austenite, F - ferrite, C- cementite, (fs, ts) point on C-curve when 1% of volume has changed phase (start of phase change), (fe, te) point on C-curve when 99% of volume has changed phase (end of phase change)

If the temperature of a steel has reached at least Ac1 temperature and then is cooled down, transformation can occur. In finite element method to calculate phase change, the transformation start can be calculated using the ideal Scheil's additivity rule, i.e. the cooling curve is divided into small isothermal time steps Δt(T) and the estimate for 1% transformation is calculated when the sum in Eq.7.1 equals unity.

$$\sum \frac{\Delta t(T)}{t_{1\%}} = 1 \tag{7.1}$$

When transformation has started, constants n(T) and k(T) are calculated [5]

$$n(T) = \frac{ln\left[\frac{ln(1-f_s)}{ln(1-f_e)}\right]}{ln(t_s/t_e)} \tag{7.2}$$

$$k(T) = \frac{-ln(1-f_s)}{t_s^{n(T)}} \tag{7.3}$$

Avrami type equation 7.4 gives the fraction of transformed material after a hold time at a given temperature:

$$f(t) = 1 - e^{-k(T)t^{n(T)}} \tag{7.4}$$

To use it in finite element method, equation 7.4 is differentiated and we obtain form:

$$\Delta f_i = (k(T)n(T)t^{n(T)-1}e^{-k(T)t^{n(T)}})\Delta t_i \tag{7.5}$$

to calculate the final fraction f

$$f = \Sigma \Delta f_i \tag{7.6}$$

References

[1] P. G. Agarwal. Eddy current losses in solid and laminated iron,. AIEE Trans, 78:169–181, May 1959.

[2] O. Biro and K. Preis. On the use of the magnetic vector potential in the finite element analysis of three-dimensional eddy currents. IEEE Trans. Magn., 25:3145–3159, July, 1989.

[3] G. Meunier C. Guerin and G. Tanneau. Surface impedance for 3D nonlinear eddy current problems—Application to loss computation in transformers. IEEE Trans. Magn., 32:808–811, May 1996.

[4] S. H. Ward D. F. Pridmore, G. W. Hohmann and W. FL Sill. An investigation of finite- element modeling for electrical and electromagnetic data in three dimensions . Geophysics, 46:1009–1024, July, 1981.

[5] Y. Rong J. Yuan, J. Kang and Jr. R.D. Sisson. FEM Modeling of Induction Hardening Processes in Steel. Journal of Materials Engineering and Performance, 12(5):589–596, 2003.

[6] D. Lowther and E. Wyatt. The computation of eddy current losses in solid iron under various surface conditions. Compumag Conf, 7, Oxford, 1976.

[7] W. Mai and G. Henneberger. Field and temperature calculations in transverse flux inductive heating devices heating nonparamagnetic materials using surface impedance formulations for nonlinear eddy-current problems. IEEE Trans. Magn., 35:1590–1593, May 1999.

[8] J. Nerg and J. Partanen. A Simplified FEM Based Calculation Model for 3-D Induction Heating Problems Using Surface Impedance Formulations. IEEE Trans. Magn., 37:3719–3722, septemper, 2001.

Coupling algorithms

zCENOS Induction Heating couples electromagnetic (harmonic) and thermal (transient or steady-state) calculations. The software allows users to choose between two coupling algorithms or allow the software to make this selection automatically.

Weak coupling (Fast calculation algorithm)

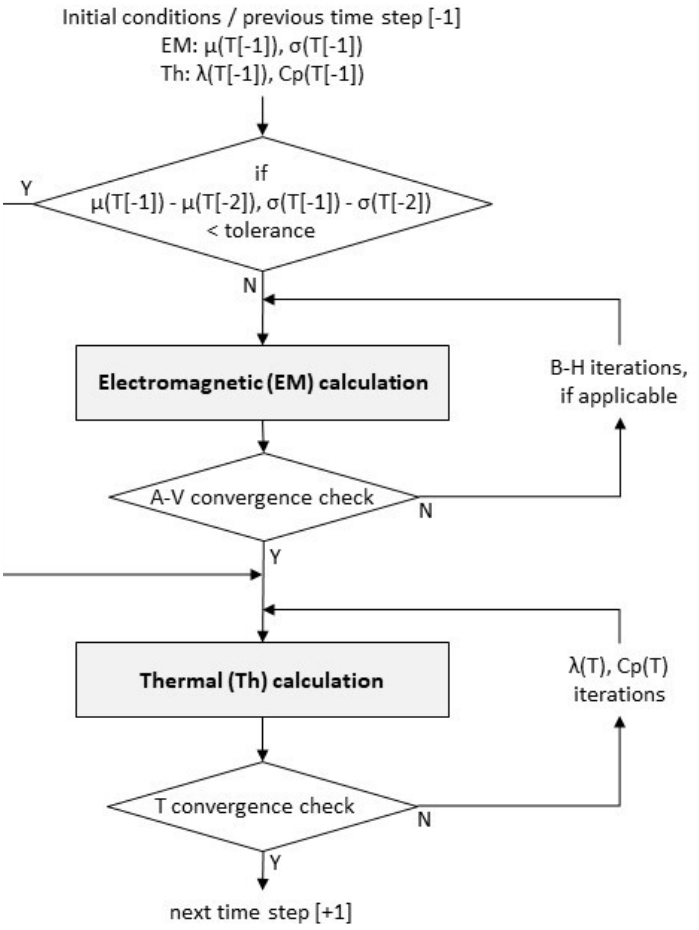

Thermal (Th) calculation follows an electromagnetic (EM) calculation, then to the next time step. There is no iterative loop between EM and Th.

If from time step to the next one, the changes in temperature dependent magnetic permeability and electric conductivity are small (less than tolerance), the algorithm skips EM calculation at this time step.

The algorithm is called “Fast” because it allows a user to get results quickly. Accuracy of the results increases with smaller time step.

Strong coupling (Accurate calculation algorithm)

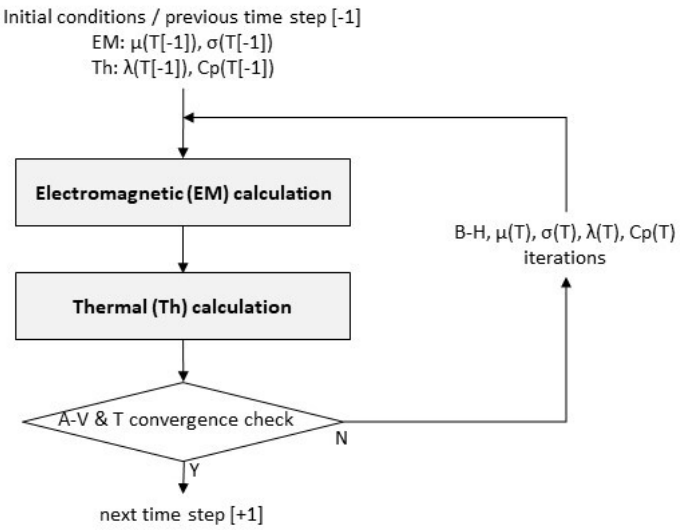

According to this algorithm, there is an iterative loop within each time step to converge all non-linear parameters: B-H, temperature dependent magnetic permeability, electrical and thermal conductivities, heat capacity.

The convergence might be slow, therefore this algorithm usually takes longer time to get to the result. However, the result is very accurate even for the course time step. Therefore, the algorithm is called “Accurate”.

Linearization of nonlinear properties

For better convergence, radiation thermal boundary condition, temperature dependent heat capacity, thermal and electric conductivities are linearized in vicinity of the current value while calculating.

For linearization (integration) of B-H curve for ferromagnetics,
https://documentation.cenos-platform.com/docs/explained/material-props
#treatment-of-non-linear-magnetic-properties-in-harmonic-ac-simulation

Hardening zone

The hardening zone filter visualizes the area which was heated above the threshold temperature during the heating process. The threshold temperature is equal to austenization temperature defined by a user for particular material.